

A Comparative Numerical Study on GEM, MHSP and MSGC

Purba Bhattacharya*, Supratik Mukhopadhyay, Nayana Majumdar, Sudeb Bhattacharya

*Applied Nuclear Physics Division, Saha Institute of Nuclear Physics,
1/AF, Bidhannagar, Kolkata 700064, India*

E-mail: purba.bhattacharya@saha.ac.in

ABSTRACT: In this work, we have tried to develop a detailed understanding of the physical processes occurring in those variants of Micro Pattern Gas Detectors (MPGDs) that share micro hole and micro strip geometry, like GEM, MHSP and MSGC etc. Some of the important and fundamental characteristics of these detectors such as gain, transparency, efficiency and their operational dependence on different device parameters have been estimated following detailed numerical simulation of the detector dynamics. We have used a relatively new simulation framework developed especially for the MPGDs that combines packages such as GARFIELD, neBEM, MAGBOLTZ and HEED. The results compare closely with the available experimental data. This suggests the efficacy of the framework to model the intricacies of these micro-structured detectors in addition to providing insight into their inherent complex dynamical processes.

KEYWORDS: Gaseous detectors; Detector modelling and simulations II (electric fields, charge transport, multiplication and induction, pulse formation, electron emission, etc); Micropattern gaseous detectors(MSGC, GEM, THGEM, RETHGEM, MHSP, MICROPIC, MICROMEGAS, InGrid, etc).

*Corresponding author

Contents

1. Introduction	1
2. Geometry Modelling	2
3. Results and Discussions	2
3.1 Electrostatic Configuration	2
3.2 Electron Collection Efficiency	4
3.3 Gain	6
3.4 Comparison between RKF results and MC results	8
4. Conclusion	8

1. Introduction

Micro Pattern Gas Detectors (MPGDs) [1], a recent addition to the gas detector family that utilize semiconductor fabrication techniques, have found wide applications in different experiments involving astro-particle physics, high energy physics, rare event detection, radiation imaging etc. Despite the widespread acceptance of MPGDs, a thorough understanding of their working principle is yet to be achieved.

In this paper we have used numerical simulation [2] as a tool of exploration to evaluate fundamental features of a MHSP detector [3]. In the process we have also simulated a GEM [4] and a MSGC [5], having similar geometrical and material features. A comprehensive comparison of their characteristics, achieved through the design variation among these detectors, have been presented. The study includes extensive computation of electrostatic field configuration within a given device and its variation for different voltage settings. Some of the fundamental properties like gain, collection efficiency have been estimated too, although of a preliminary nature at present, and compared to the reported experimental results.

We have used the recently developed simulation framework Garfield [6, 7] that combines packages such as neBEM [8–11], Magboltz [12, 13] and Heed [14, 15]. It may be mentioned here that the simulation framework used in this work was augmented in 2009 through the addition of the neBEM toolkit to carry out 3D electrostatic field simulation. Earlier, Garfield had to import field-maps from one of the several commercial FEM packages in order to study 3D gas detectors. Due to the exact foundation expressions based on the Green's functions, the neBEM approach has been found to be exceptionally accurate in the complete physical domain, including the near field. This fact, in addition to other generic advantages of BEM over FEM, makes neBEM a strong candidate as a field-solver for MPGD related computations. Some of the major generic advantages of BEM are its ability to estimate the field directly and to handle open geometries. FEM also has

several advantages to its credit, such as flexibility, ability to simulate non-linear problems and huge popularity. While the Garfield + neBEM framework has been applied for modelling Micromegas detectors on several occasions [16, 17], very few reports are available for detectors having a fair amount of dielectric material, such as MSGC, GEM or MHSP.

2. Geometry Modelling

A schematic drawing to represent a MHSP has been depicted in the figure 1(a). Basically a MHSP merges the MSGC and the GEM features in a single, double-sided element. The top surface looks similar to a GEM (figure 1(c)). The bottom plane (figure 1(b)) is etched for parallel anode (A) and cathode (C) strips (quite similar to a MSGC shown in figure 1(d)) with holes within the cathode strips (unlike in a MSGC where there are no holes). The anode and cathode strips in the MHSP (also for the MSGC) are kept at a potential difference, V_{ac} , while that across a hole between the top grid (denoted by T) and the cathode at the bottom is V_h for both MHSP and GEM. Figure 1(a) also depicts the potential difference applied in the drift region, V_{drift} . Similarly, a potential difference in the induction region, V_{ind} is also maintained. Corresponding electric fields are denoted by E_{drift} and E_{ind} , respectively. It may be mentioned here that for the MSGC there is no induction region. Two stages of amplification of electrons in a MHSP have been denoted in figure 1(a) as g_h and g_s which represent the multiplication inside the hole and that near the strips, respectively. The design parameters, considered in the numerical work, are mentioned in table 1.

Table 1. Design Parameters

	MHSP ([18])	GEM ([18 – 20])	MSGC (similar to MHSP)
Polymer substrate (P) thickness	50 μm	50 μm	50 μm
copper coating thickness	5 μm	5 μm	5 μm
hole diameter in the copper layer	70 μm	70 μm	
hole diameter at the middle of the Polymer substrate	50 μm	50 μm	
hole to hole pitch (Y direction)	140 μm	140 μm	
anode width	15 μm		15 μm
cathode width	100 μm		100 μm
anode to cathode gap (edge to edge)	30 μm		30 μm
anode to anode pitch	175 μm		175 μm

3. Results and Discussions

3.1 Electrostatic Configuration

Figure 2(a) presents the variation of the total electric field along the hole axis of the MHSP for different V_{ac} and a fixed V_h . A comparison with the GEM total field reveals that, for the same V_h ,

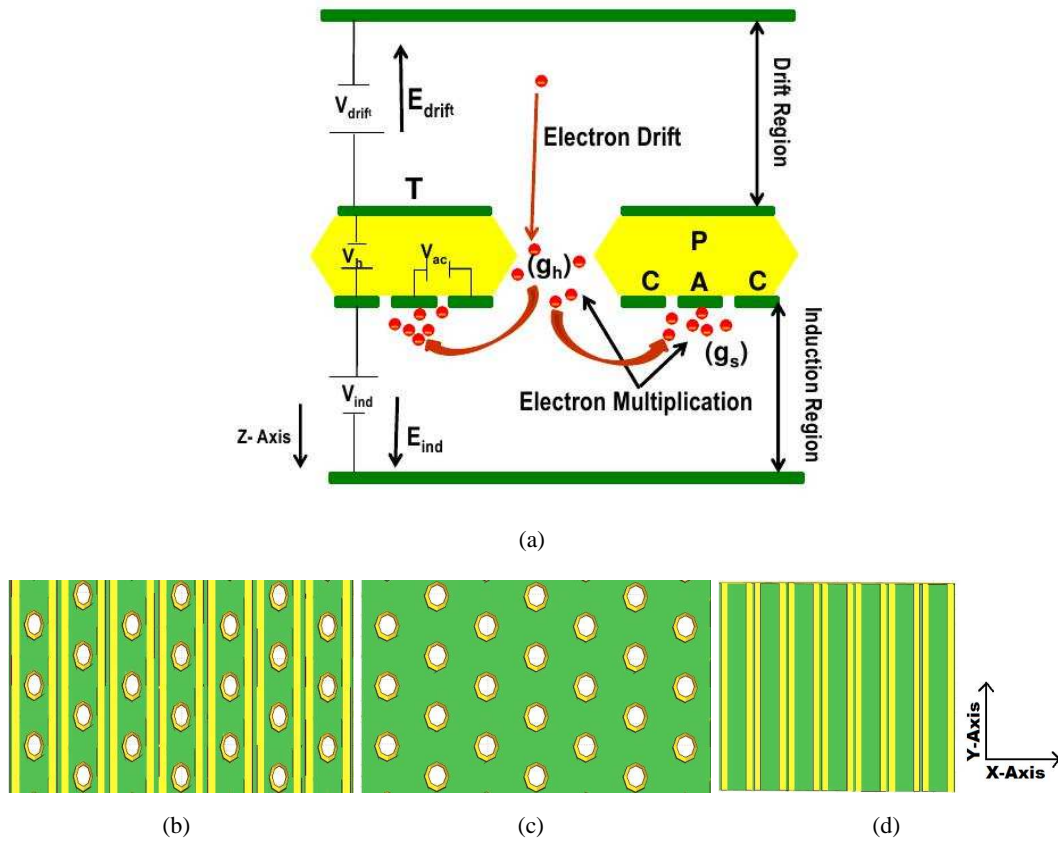


Figure 1. (a) Schematic representation for MHSP, (b) Lower surface of MHSP (c) GEM, (d) MSGC

the fields for MHSP and GEM can be made identical by assigning $V_{ac} = 0$ V. Thus it is possible to operate the MHSP in a GEM mode. It can be also noted that an increase in V_{ac} does not affect the maximum value of the field.

One of the main differences between a GEM and a MHSP detector is that for the GEM, the voltage applied on the bottom induction plane is positive with respect to the bottom grid surface, so that on the emergence from the hole, the electrons drift towards the induction plane where they are collected. But in the case of a MHSP, the induction plane voltage is negatively biased with respect to the bottom cathode strips voltage. As a result the electrons are deflected towards the anode strips. The field in the induction region for a GEM is higher than that for a MHSP.

Figure 2(b) compares the field lines passing through the hole center with two off-center lines along the z-direction. From this figure it is seen that as we proceed towards the edge of the hole, the smooth nature of the field is distorted by sharp gradients.

Figure 3(a) shows that the field near the grid surface (T) and in the immediate proximity of the hole entrance is also not influenced by V_{ac} and is same as the top surface of a GEM. If we increase the V_{ac} from 0 V to 220 V, the change in the value of the electric field is only 5 %. A similar observation was also made for Reverse-MHSP [21]. But a change in V_h has a direct impact on this field (Figure 3(b)). Thus the electron focusing into MHSP holes are not affected much by V_{ac} and can be studied as a function of V_h only.

In figure 4 we have depicted the variation of the potential and the electric field on the Micro

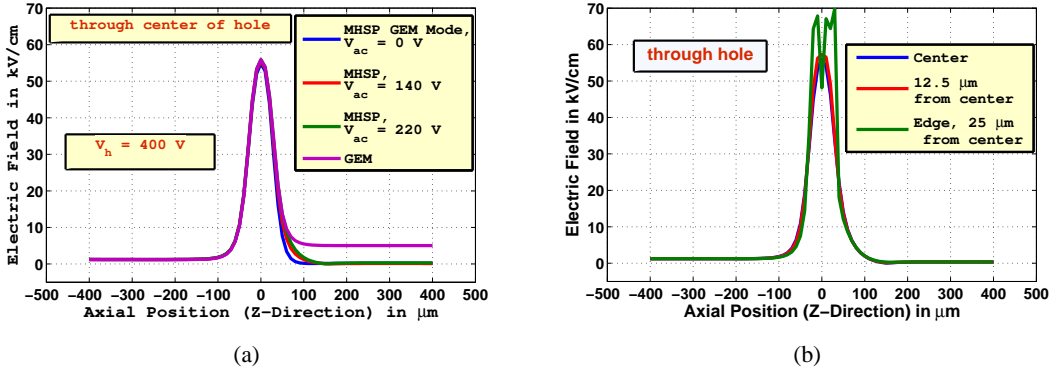


Figure 2. (a) Comparison of the total electric field of a MHSP and a GEM along the axial lines passing through the hole center for a fixed V_h and different V_{ac} , (b) Total electric field of a MHSP along an axial line passing through the hole center and two off-center lines along z-direction

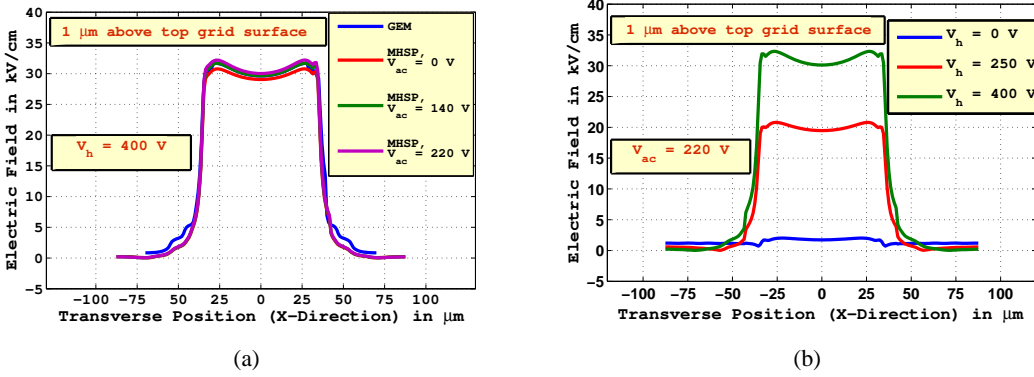


Figure 3. Variation of the electric field in the immediate proximity of the hole entrance due to the change of (a) V_{ac} for a fixed V_h , (b) V_h for a fixed V_{ac}

Strip surface of a MHSP due to variation in V_h for a fixed V_{ac} . Without any hole voltage, the bottom microstrip surface of the MHSP, acts as an ordinary MSGC. It is further observed that potential and field are both strongly affected by a variation in V_h . As a result, the multiplication factor in second amplification stage (g_s) and the collection efficiency of the anode not only depends on V_{ac} , but also on V_h .

3.2 Electron Collection Efficiency

An Ar – CO₂ gas mixture (70 : 30) at 293 K and 1 atmosphere has been considered here. We have defined two tracks of primary-ionization electrons in the drift region: 1) a set of 30 electrons starting at 240 μm above the MHSP top grid and 2) a set of 20 electrons starting at a position 1 μm above the grid. In the following discussions the drift lines are estimated using simple Runge-Kutta-Fehlberg (RKF) method and thus the electron diffusion in gas is ignored (figure 5).

Depending on the voltage settings of different electrodes, some electrons are lost on the top grid surface, dielectric and the cathode strips as shown schematically in figure 6. The variation of the electron collection efficiency of the anode with V_h for a fixed V_{ac} and with V_{ac} for a fixed V_h are

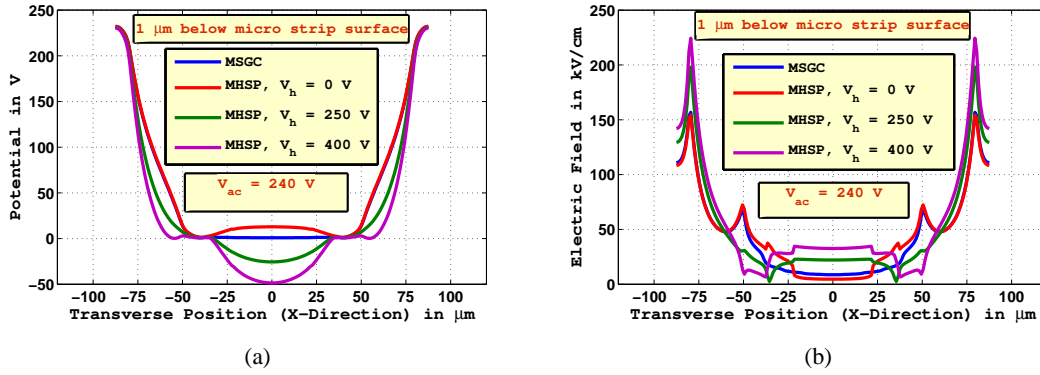


Figure 4. Effect of V_h on the (a) Potential, (b) Electric field near the micro strip surface, for a fixed V_{ac}

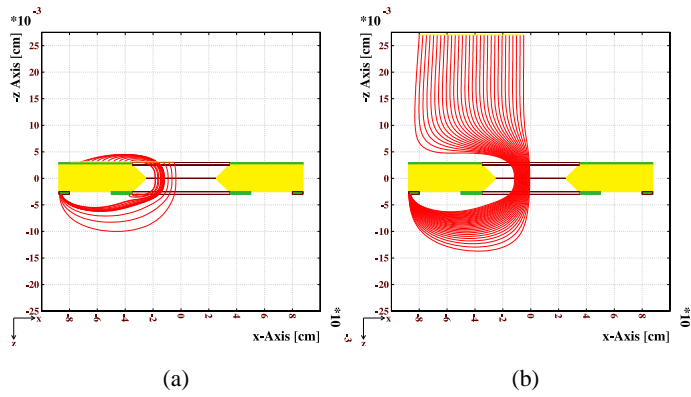


Figure 5. Electron drift lines using RKF method from pre-defined track; (a) $1 \mu\text{m}$ and (b) $240 \mu\text{m}$ above the top grid surface

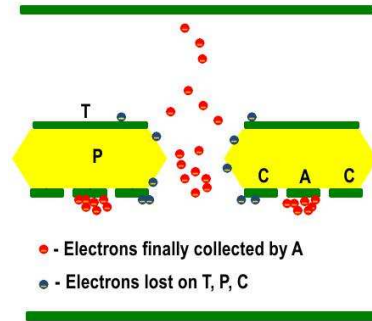


Figure 6. The end point of electrons on different electrodes for MHSP

presented in figure 7(a) and figure 7(b) respectively. Variations of V_{drift} and V_{ind} is also expected to affect the parameter, but have not been considered in the present study. For a fixed V_{ac} , a minimum V_h is required to focus the electrons towards the hole, otherwise the electrons are lost on the top of the grid surface. Beyond a certain V_h all the electrons are focused towards the hole and finally collected by the anode strips. But if we increase the V_h even more, some of the electrons which start their journey close to the grid surface (mainly the electrons whose drift paths are near the

edge of the hole) end their journey at the cathode strips (figure 8(a)) since for them the anode strips voltage is not sufficient to pull them. As a result, the efficiency drops (blue lines in figure 7(a)). We can increase this efficiency once again by increasing V_{ac} (blue line in figure 7(b), since for a particular V_h , increase of the V_{ac} attracts the electrons more towards the anode strip (figure 8(b)).

The electrons which start their journey in the middle of the drift region, mainly drift through the central part of the hole. So most of these electrons reach the anode strips safely (red lines of Figure 7(a) and figure 7(b)).

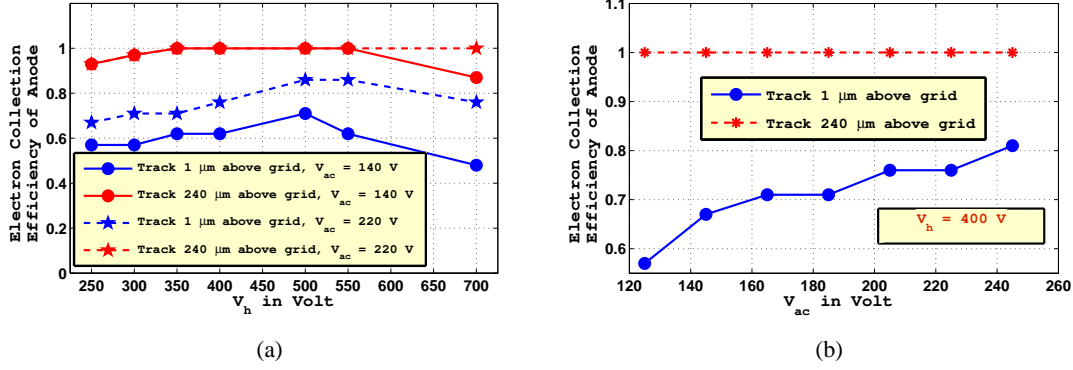


Figure 7. Variation of electron collection efficiency of anode, (a) with V_h (b) with V_{ac}

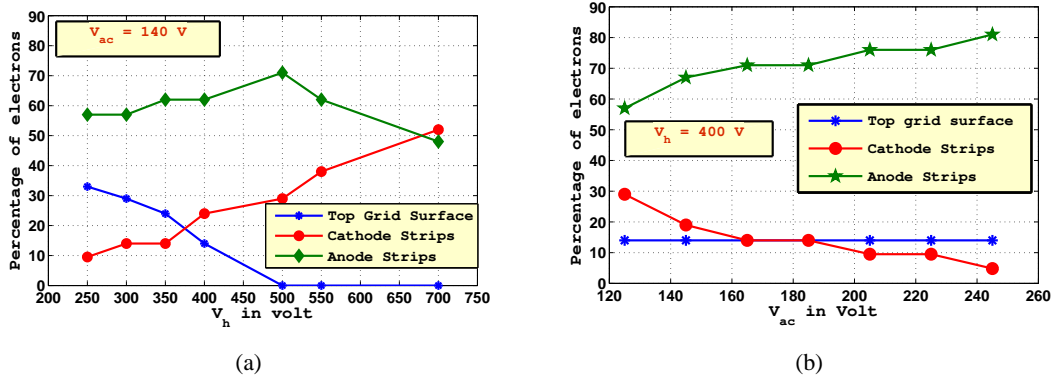


Figure 8. Percentage of electrons collected on different electrodes, (a) dependence on V_h for a fixed V_{ac} , (b) dependence on V_{ac} for a fixed V_h

From the above graphs, it is seen that the electron collection efficiency can be maximized with proper optimization of V_h and V_{ac} . For this particular geometry, a V_h of 500 V is suitable (collection efficiency 80 %) for two sets of V_{ac} (140 V and 220 V), studied here. At this value of V_h , an increase of V_{ac} certainly improves the efficiency, but this choice of voltage is likely to be governed by the sparking limit.

3.3 Gain

The effective gain of electrons for a particular track is obtained as

$$g_{\text{eff}} = \epsilon_{\text{prim}} \times g_{\text{mult}} \times \epsilon_{\text{sec}} \quad (3.1)$$

where ϵ_{prim} is the primary electron collection efficiency and is the probability for a primary electron to reach the hole region. g_{mult} is the multiplication factor of the electrons throughout their trajectories. For a GEM, the multiplication occurs only inside the hole (g_{h} in figure 1(a) and thus, $g_{\text{mult}} = g_{\text{h}}$). In case of MSGC, V_{ac} is responsible for the electron multiplication near the micro strip surface ($g_{\text{mult}} = g_{\text{s}}$). As designed, the MHSP combines these two stages of multiplication (figure 1(a)). So in this case, $g_{\text{mult}} = g_{\text{h}} \times g_{\text{s}}$. ϵ_{sec} is the secondary electron collection efficiency of the readout electrode. It may be noted here that we have considered only the collected charge at the anode strips (A) to determine effective gain .

The discussion in the previous section suggests that electrons arising from different positions of the drift region behave quite differently. Since in an experiment, the gamma rays from a radiation source can liberate the primary electrons in different parts of the drift region, we choose four tracks at different distances above the top grid surface ($1 \mu\text{m}$, $10 \mu\text{m}$, $500 \mu\text{m}$ and 1 mm). The total gain (g_{t}) is the average effective gain of the electrons from these four tracks.

The gas mixture considered in this work is a Penning mixture. After considering results using two transfer rates, 56% (extrapolated value from [22]) and 70% (a guess work), we chose to carry out the rest of the calculations with the higher value since it agreed well with the experimental data. This issue, however, needs further investigation.

The variation of the gain (g_{t}) with V_{h} for a GEM, is shown in figure 9(a). For a MHSP, the same variation of g_{t} is depicted in figure 9(b). When the MHSP is operated in a GEM mode ($V_{\text{ac}} = 0 \text{ V}$, $g_{\text{s}} = 1$ and thus $g_{\text{mult}} = g_{\text{h}}$), g_{t} is similar to that obtained with a single GEM. But for the same variation of V_{h} , g_{t} increases with the increase of V_{ac} . The trend obtained from the present simulated estimates is similar to that observed in experiment by Veloso et al. [24].

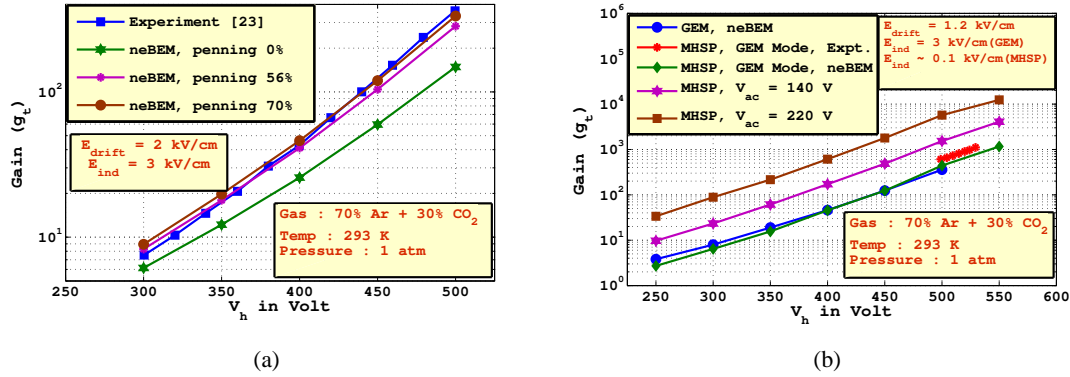


Figure 9. Variation of g_{t} with V_{h} under different conditions for (a) GEM , (b) MHSP

In Figure 10(a), we present the variation in g_{t} due to variation in V_{ac} for a fixed V_{h} . Since, the gain for this fixed V_{h} can be calculated from the above procedure (MHSP in GEM mode) we can make a rough estimate of the gain ($g_{\text{mult}} = g_{\text{s}}$) in the 2nd amplification stages only. The experimental results [18] verify this nature.

Experimentally it was considered in the work of Veloso et al. [3] that a fraction of the incident X-rays can interact in the induction region, below the MHSP. The primary electron clouds from these events experience only one stage of charge multiplication at the micro strip anodes ($g_{\text{mult}} = g_{\text{s}}, g_{\text{h}} = 1$). When $V_{\text{h}} = 0 \text{ V}$, no electrons from the drift region can reach the micro

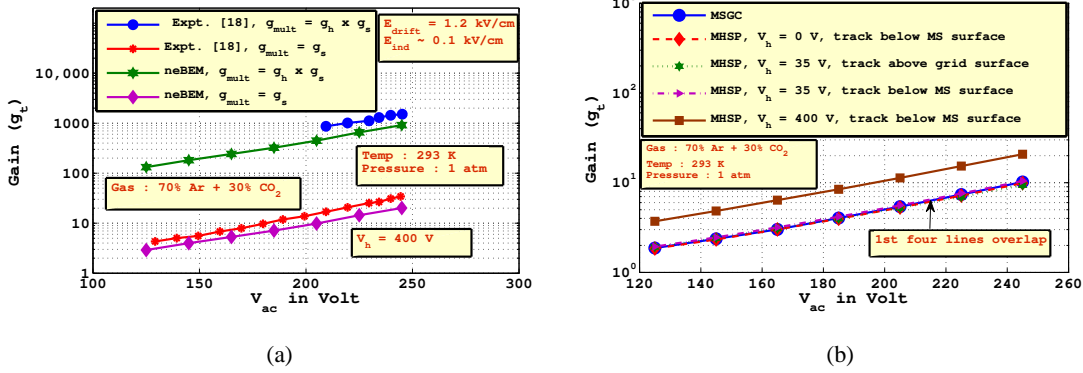


Figure 10. Variation of g_t with V_{ac} under different conditions

strip surface and in this case, g_t of a MHSP is of the same order of a single MSGC, as shown in the Figure 10(b). When V_h is adequate for only electron transmission, but not for hole multiplication (for example, $V_h = 35$ V), then also the amplification factor of electrons from above or below the MHSP depend only on V_{ac} . The gain (g_t) of the above four graphs in figure 10(b) is of the same order. But V_h beyond a certain value has an effect not only on the electric field inside the hole but also on the micro strip surface (figure 4) which affects g_s and thus g_t . In this situation ($V_h = 400$ V in figure 10(b)), g_t is higher than that of above four graphs, but of the same order as obtained in figure 10(a) (red and purple line).

From the above gain study, it is seen that the total gain of a MHSP depends on the potential difference of two different amplification stages. With proper optimization of V_h and V_{ac} , the total gain of MHSP can be made higher than that of a single GEM or a MSGC.

3.4 Comparison between RKF results and MC results

The electron trajectories using Monte-Carlo (MC) technique that takes diffusion into account is shown in figure 11(a). It is expected and observed that the loss of electrons on different electrodes increases due to diffusion which naturally affects ϵ_{prim} and ϵ_{sec} . Figure 11(b) and figure 11(c) shows the variation of ϵ_{prim} and ϵ_{sec} respectively with V_{ac} for a fixed V_h . A more realistic MC calculation yields a smaller efficiency than simple RKF method and thus a smaller value of gain as presented in figure 11(d). It is to be noted that in both the RKF and MC calculations, charge induction effects of moving electrons have not been considered. Inclusion of these effects while estimating total gain is expected to bring the MC estimates much closer to the measured values.

4. Conclusion

We have used Garfield+neBEM+Magboltz+Heed combination to simulate the physical processes and the performance of a MHSP detector having realistic dimensions. A detailed study of the parametric variation of the 3D electric field, detector gain, collection efficiency has been carried out. It has been observed that while electron focusing in a MHSP detector is almost entirely dependent on the hole voltage, its gain and electron collection efficiency requires optimum combination of both hole and strip voltages. The well regarded but simplistic RKF method has provided quite

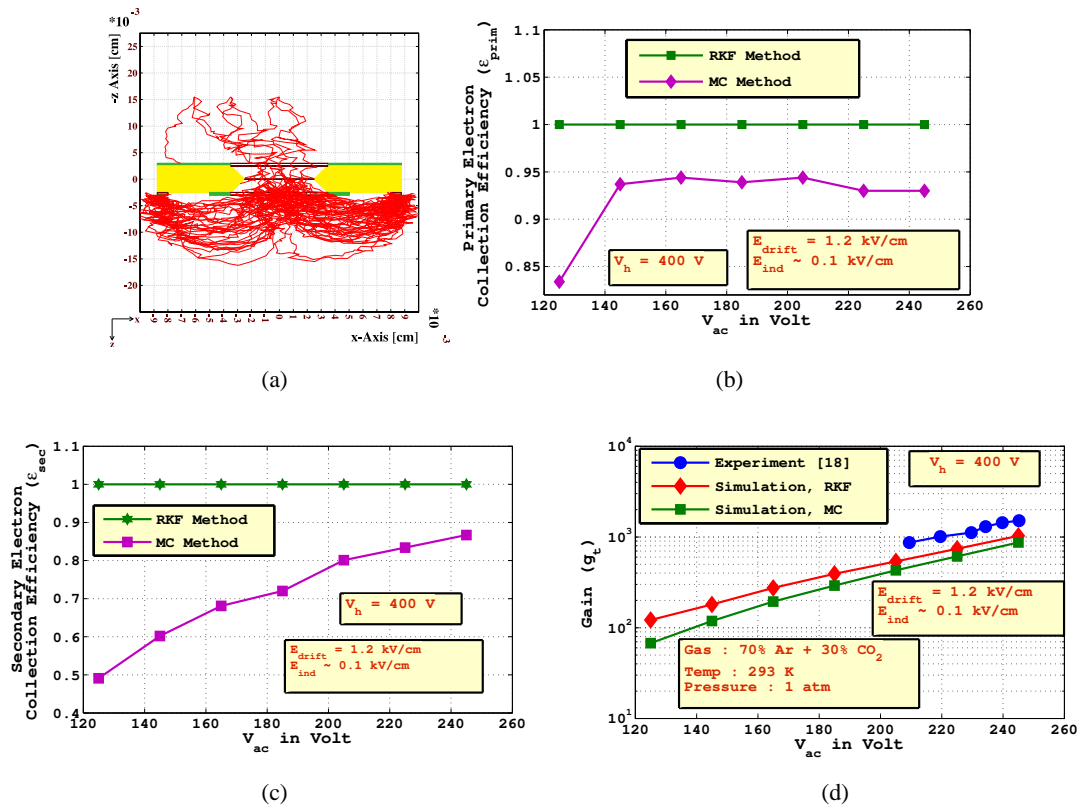


Figure 11. (a) Electron Drift line using MC Method, Variation of (b) ϵ_{prim} , (c) ϵ_{sec} , (d) g_t with V_{ac} for a fixed V_h

acceptable results in the present studies. However, as demonstrated, MC simulation, incorporating the effects of diffusion, promises more realistic results. The overall trend observed in the above studies has been found to be in agreement with the existing experimental results. The comparative study highlights the advantages of a single MHSP detector over single GEM or MSGC. On the one hand, while carrying out the computations we felt the necessity to have more experimental details than are available in the published literature. On the other hand, important details such as induced component of the signal, space charge and charging up effects, estimates of manufacturing tolerances and defects have been left out of the present computations. In future, we hope to make progress in all these areas in order to achieve an even better understanding of these devices.

Acknowledgments

This work has partly been performed in the framework of the RD51 Collaboration. We happily acknowledge the help and suggestions of the members of the RD51 Collaboration. We also thank the reviewers for their valuable comments.

References

- [1] P. Fonte and V. Peskov, *On the Physics and technology of gaseous particle detectors, Plasma Sources Sci. Technol.* **19** (2010) 034021.

- [2] R. Veenhof, *Numerical methods in the simulation of gas-based detectors*, 2009 *JINST* **4** P12017.
- [3] J.F.C.A. Veloso, J.M. Maia, R.E. Morgado, J.M.F. dos Santos, C.A.N. Conde, *The microhole and strip plate gas detector: Initial results*, *Rev. Sci. Instrum.*, **73** (2002) 488.
- [4] F. Sauli, *GEM: A new concept for electron amplification in gas detectors*, *Nucl. Instrum. Meth.*, **A 386** (1997) 531.
- [5] A. Oed, *Position-sensitive detector with microstrip anode for electron multiplication with gases*, *Nucl. Instrum. Meth.* **A 263** (1988) 351.
- [6] R. Veenhof, *Garfield - Simulation of gaseous detectors*, online at <http://cern.ch/garfield>.
- [7] R. Veenhof, *Garfield, recent developments*, *Nucl. Instrum. Meth.*, **A 419** (1998) 726.
- [8] S. Mukhopadhyay and N. Majumdar, *A nearly exact Boundary Element Method*, online at <http://cern.ch/neBEM>.
- [9] N. Majumdar and S. Mukhopadhyay, *Simulation of three dimensional electrostatic field configuration in wire chambers: A novel approach*, *Nucl. Instrum. Meth.*, **A 566** (2006) 489.
- [10] S. Mukhopadhyay and N. Majumdar, *Computation of 3D MEMS electrostatics using a nearly exact BEM solver*, *Eng. Anal. Boundary Elem.*, **30** (2006) 687.
- [11] S. Mukhopadhyay and N. Majumdar, *A study of three dimensional edge and corner problems using the neBEM solver*, *Eng. Anal. Boundary Elem.*, **33** (2009) 105.
- [12] S. Biagi, *Magboltz - Transport of electrons in gas mixture*, online at <http://cern.ch/magboltz>.
- [13] S.F. Biagi, *Monte Carlo Simulation of electron drift and diffusion in counting gases under the influence of electric and magnetic field*, *Nucl. Instrum. Meth.*, **A 421** (1999) 234.
- [14] I. Smirnov, *Interactions of particles with gases*, online at <http://cern.ch/heed>.
- [15] I.B. Smirnov, *Modeling of ionization produced by fast charged particles in gases*, *Nucl. Instrum. Meth.*, **A 554** (2005) 474.
- [16] P. Bhattacharya, S. Mukhopadhyay, N. Majumdar, S. Bhattacharya, *Realistic three dimensional simulation on the performance of micromegas*, *Nucl. Instrum. Meth.*, **A 628** (2011) 465.
- [17] K. Nikolopoulos, P. Bhattacharya, V. Chernyatin and R. Veenhof, *Electron transparency of a MicroMEGAS mesh*, 2011 *JINST* **6** P06011.
- [18] J.M. Maia, J.F.C.A. Veloso, J.M.F. dos Santos, A. Breskin, R. Chechik, D. Mörmann, *Advances in the Micro-Hole & Strip Plate gaseous detector*, *Nucl. Instrum. Meth.*, **A 504** (2003) 364.
- [19] S. Bachmann, A. Bressan, L. Ropelewski, F. Sauli, A. Sharma, D. Mörmann, *Charge amplification and transfer processes in the gas electron multiplier*, *Nucl. Instrum. Meth.*, **A 438** (1999) 376.
- [20] A. Sharma, *3D simulation of charge transfer in a Gas Electron Multiplier (GEM) and comparison to experiment*, *Nucl. Instrum. Meth.*, **A 454** (2000) 267.
- [21] A.V. Lyashenko, A. Breskin, R. Chechik, J.F.C.A. Veloso, J.M.F. dos Santos and F.D. Amaro, *Advances in ion back-flow reduction in cascaded gaseous electron multipliers incorporating R-MHSP elements*, 2006 *JINST* **1** P10004.
- [22] Ö. Sahin, İ. Tapan, Emin N. Özmutlu and R. Veenhof, *Penning transfer in argon-based gas mixtures*, 2010 *JINST* **5** P05002.

- [23] G. Croci, *Development and Characterization of Micro-Pattern Gaseous Detectors for HEP application and beyond*, Ph D thesis, University of Siena (2010)
- [24] J.F.C.A. Veloso et al. , *Recent advances in X-ray detection with micro-hole and strip plate detector*, *Nucl. Instrum. Meth.*, **A 524** (2004) 124.